Separation and Purification Technology 224 (2019) 580–590

Contents lists available at ScienceDirect

Separation and Purification Technology

journal homepage: www.elsevier.com/locate/seppur

Hollow fiber gas membrane-based removal and recovery of ammonia from water in three different scales and types of modules

Philip A. Aligwe[a], Kamalesh K. Sirkar[a,*], Christian J. Canlas[b]

[a] Otto York Department of Chemical and Materials Engineering, New Jersey Institute of Technology, University Heights, Newark, NJ 07102, USA
[b] W. R. Grace, Catalysts Technologies, 7500 Grace Drive, Columbia, MD 21044, USA

A B S T R A C T

Ammonia present in many industrial process streams and effluent streams is beginning to be recovered by means of microporous hydrophobic hollow fiber-based membrane contactor devices with gas-filled pores; the process is often characterized as supported gas membrane (SGM) process. Ammonium sulfate is usually obtained in a sulfuric acid stream on the other side of the membrane. It is useful to develop a quantitative basis for the extent of ammonia removal in such devices. Unlike deoxygenation of aqueous streams in such devices, membrane resistance is quite important for ammonia transport. Ammonia transport modeling in such devices is hampered by the complexity of feed liquid flow in the shell side of commercially used devices and lack of information on membrane resistance where membrane tortuosity introduces considerable uncertainty. The approach adopted here involves studying ammonia transport with the feed solution flowing through the hollow fiber bore where the fluid mechanics is simpler than shell-side flows. Comparison of model-based predictions of overall mass transfer coefficient (k_o) with experimentally observed values allows estimation of the membrane mass transfer coefficient (k_m). One can use such estimates of k_m to model the observed ammonia transport in small crossflow devices and develop an empirical guidance of the dependences of the shell side mass transfer correlations. Guided by such information and deoxygenation SGM literature, a model was developed for large modules used for ammonia recovery via SGM. Model predictions of performances of the large modules are likely to be useful for various process considerations including the effect of temperature and feed flow rate variations on ammonia removal.

1. Introduction

Effluent streams from municipalities, industrial operations, agricultural and animal husbandry activities are the principal sources of ammonia emissions [1,2]. For removal of low concentrations of ammonium ion by ion exchange process, regeneration of the bed by an alkaline NaCl solution generates a waste stream of NH_4Cl solution requiring further treatment [3]. Ammonia present in low concentrations is often subjected to biodegradation yielding N_2 [4]. There are industrial effluent streams where ammonia concentration can be as high as 6000–8000 ppm [5]. Such streams are suitable for recovering ammonia instead of converting it to nitrogen via biodegradation [4]. The form in which ammonia exists in the effluent depends on the pH and temperature. Ammonia is present almost completely as readily strippable dissolved ammonia gas for temperatures less than 50 °C if the pH > 11; for similar temperatures, at a pH < 7, it is present almost completely as ammonium ion [6,7]. At an intermediate pH, the extent to which it exists as dissolved gas varies almost linearly with pH except at the two ends of the pH range.

Current industrial practice converts the dissolved ammonia to essentially strippable gas which is then stripped by air in a packed tower. This is implemented by raising the effluent pH to > 11 by adding alkali. Ammonia in this air stream is recovered as $(NH_4)_2SO_4$ by contacting the stripped air stream counter-currently with a sulfuric acid stream in a second packed tower.

Using a porous hydrophobic hollow fiber membrane-based contacting technique called gas membrane or supported gas membrane (SGM), a number of studies have been made [8–13] wherein ammonia is stripped from the feed aqueous solution into gas-filled pores of the membrane on the other side of which sulfuric acid reabsorbs the ammonia and produces ammonium sulfate. By means of such a technique, the two tower-based process of ammonia-stripping in one packed tower and its reabsorption in another packed tower into sulfuric acid is replaced by one device. The process is quite rapid and replaces large towers with small membrane devices having orders of magnitude larger surface area per unit device volume. Such a technique has been studied for cyanide removal as well [14–18]. An alternate name has also been proposed for such a process: TransMembraneChemiSorption (TMCS) [5,19].

The inherent strength of this process lies among others in the location of the gas-sulfuric acid solution interface only 25–50 μm (the thickness of the hollow fiber wall) apart from the location where ammonia is being stripped. This allows the possibility of reducing the treated effluent concentration of ammonia to low levels [5]. To achieve such low levels in a packed tower, one has to increase substantially the flow rate of air.

* Corresponding author.
E-mail address: sirkar@njit.edu (K.K. Sirkar).

https://doi.org/10.1016/j.seppur.2019.04.074
Received 4 March 2019; Received in revised form 22 April 2019; Accepted 22 April 2019
Available online 23 April 2019
1383-5866/

Nomenclature

a, b, c	parameters/constants in Eq. (11a)
A_c	membrane cross-sectional area
A_{fc}	actual flow cross-sectional area
A_T	transfer area between two phases in the contactor
C	total ammonia concentration in feed solution
C_o	total ammonia inlet concentration
C_{out}	total outlet concentration of ammonia
C_i	concentration of species i in the bulk solution (i: 1 = NH_3; 2 = NH_4^+; 3 = OH^-; 4 = H_2O; 5 = H_2SO_4; 6 = Air)
C^{eq}	concentration of ammonia in equilibrium with sulfuric acid
d_i	inner diameter of hollow fiber
d_f	outer diameter of hollow fiber
d_p	pore diameter
D_i	diffusion coefficient of species i in the bulk solution
$D_{g,e}$	effective diffusion coefficient of NH_3 gas through gas-filled pores
$D_{g,k}$	Knudsen diffusion coefficient of NH_3 gas through gas-filled pores
E	NH_3 gas removal efficiency in the contactor
f_X	fractional open area for flow of liquid (in the radial plane, inward or outward)
f_p	packing fraction of hollow fibers
Gr	Graetz number, $((\pi (d_i)^2/4)\ v/(D_i\ L))$
h	contribution factor of ionic/gaseous species in solution towards the effective Henry's constant
H	Henry's constant in H_2O
H_{eff}	effective Henry's constant in H_2O
J	total ammonia flux
k_f	feed mass transfer coefficient
k_m	membrane mass transfer coefficient
k_o	overall mass transfer coefficient
K	base dissociation constant of ammonia
L	effective hollow fiber length in the module
M_i	molecular weight of species i
n_f	number of fiber layers in crossflow direction
N	total number of hollow fibers
Q	feed volumetric flow rate
r	radius of differential slice
R_{ci}	inner radius of cartridge
R_{co}	outer radius of cartridge
R_i	inner radius of hollow fiber
R_o	outer radius of hollow fiber
R	universal gas constant
t	membrane thickness
T	temperature
v	axial velocity through the bore/lumen of a hollow fiber
v_r	local radial velocity on the shell side at radius r
v_x	local axial velocity on the shell side at distance x
W	length of hollow fiber perpendicular to feed solution in cross flow
z	vertical location of ammonia concentration in the module
ε	membrane porosity
Λ	composite transport property parameter, defined by Eq. (11d)
ρ	density of liquid
τ	membrane tortuosity
μ	viscosity of liquid

The hollow fiber membrane device used in such processes can be quite large having a surface area of as much as 130 m^2 [5]. The flow configurations of the two liquid streams in such devices are of considerable importance insofar as various mass transfer resistances are concerned. Since the sulfuric acid stream used is quite concentrated and ammonia absorption rate into it is very high, the mass transfer resistance on the sulfuric acid side is usually neglected. There are two other resistances, that on the liquid feed side and that through the porous hydrophobic membrane. In the stripping of low solubility gases such as oxygen, the aqueous phase mass transfer resistance is controlling compared to that through the gas phase in membrane pores. Since crossflow over the outside of hollow fibers enables achievement of high liquid phase mass transfer coefficients, the liquid subjected to gas desorption is designed to flow on the shell-side over the hollow fibers in crossflow [20–22].

Therefore in large hollow fiber modules used for deoxygenation of water, the feed aqueous phase containing the dissolved oxygen species flows on the shell side in crossflow over the outside of the hollow fibers [23]. Such a process provides high shell-side mass transfer coefficients at low cross-flow Reynolds numbers around the hollow fibers incurring a low pressure drop in the feed liquid flow. For designing the performance of such modules in general, one can use conveniently the approach of addition of three resistances in series, feed liquid film resistance, gas membrane resistance and strip-side sulfuric acid film resistance. The last one may be neglected. This model has to be integrated with the overall module flow configuration, detailed module design and porous membrane information.

For deoxygenation using vacuum and N_2 gas sweep on the strip side (fiber bore) and aqueous phase cross-flow on the shell side, a semi-empirical model was developed to successfully predict the deoxygenation performance of large cross-flow modules [23]. The power of the shell-side Reynolds number in the mass transfer correlation was empirically determined from the best fit with experimental deoxygenation data. The model prediction in terms of fractional deoxygenation bypassed the need for an exact mass transfer correlation of the liquid in cross flow over the hollow fibers on the shell side. This was possible because the membrane mass transfer resistance is not important in deoxygenation. However, in the case of ammonia removal, the membrane mass transfer resistance becomes very important and one needs a good correlation for the feed side mass transfer coefficient.

Larger size devices used in this application employ large-size LiquiCel® module with a baffle in between to introduce countercurrent configuration with local crossflow. Zheng et al. [24] have proposed a correlation for the shell-side liquid flow with considerable details. Others who have modeled ammonia transfer using gas membranes include the following references [10,13]. Both of these studies did not employ crossflow on the shell side and employed smaller modules. Further, the feed solution was flowing through the tube-side. The study in [10] employed a buffered feed solution whereas the study in [13] employed high pH by adding caustic soda. In industrial practice, the pH is usually raised quite high so that almost all of the ammonia is present in the form of dissolved gas.

The approach taken here in understanding the performance of such systems is to study a number of module configurations and dimensions to develop a usable basis for predictive capability. We have measured the ammonia transfer rate in two types of smaller modules. In the smallest modules identified as MicroModule™, (membrane area, 98.9 cm^2), we have crossflow of the ammonia-containing feed liquid over the porous hydrophobic hollow fibers with the sulfuric acid stream flowing through the fiber bore. In another larger cylindrical hollow fiber module (MiniModule™), (membrane area, ~1800 cm^2), we have parallel flow of both liquid streams with the ammonia-containing feed liquid flowing through the hollow fiber bore. The latter involves a situation where the feed side mass transfer regime is characterized somewhat more easily.

Problems in developing predictive capability for membrane

contactor module performances generally arise due to the problems of predicting the liquid side mass transfer resistance for liquid flow in the shell-side and the membrane resistance. In cases where the membrane resistance is negligible as in deoxygenation of water flowing in the shell-side, it appears that there is some progress [23,24]. However, the literature does provide an array of correlations; some involve SGM systems (see Estay et al. [25]). In cases where membrane resistance is important, it is preferable to estimate it from experiments. One can approach the problem in two ways. For the MiniModules™ with feed flow through the hollow fiber bore, one can assume that feed liquid transfer coefficient is more easily obtained and therefore experimental data may be used to estimate membrane resistance. Then one can use such a value of membrane resistance to find out how the shell-side liquid film resistance is behaving in crossflow systems of the MicroModule™. Alternately, one can employ theoretical estimates of membrane resistance and find out how the models developed for the two configurations describe the observed behavior.

If one can achieve a reasonable predictive capability in the two smaller configurations studied here with two different feed liquid flow configurations, then we can take the following step. It is assumed that one can combine the shell-side flow model from Sengupta et al. [23] and the shell-side mass transfer correlation of Zheng et al. [24] and develop a reasonable predictive capability for the much larger LiquiCel® modules after incorporation of membrane resistance. Modeling performances of larger 10 × 28 modules from literature using the shell-side flow correlation from [24] is thus of significant interest here.

2. Experimental

2.1. Materials and chemicals

Ammonium hydroxide (NH_4OH) (35.046 g/mol, 28–30%, Fisher, Hanover Park, IL); ammonium chloride (NH_4Cl) (53.49 g/mol, ≥99.0%, Fisher, Hanover Park, IL); sodium hydroxide (Fisher). Microporous hydrophobic polypropylene hollow fibers were used in the modules for the experiments. Table 1 provides various details of a 0.5 × 1 Micromodule™ and a 1 × 5.5 MiniModule™ provided by 3 M (Charlotte, NC, USA). Table 1 also provides information on the large 10x28 modules used in industrial operations.

2.2. Methods

The schematic of the setup used for transport studies conducted with the 0.5 × 1 MicroModule™ is shown in Fig. 1. Ammonia-containing feed solution was prepared by adding NH_4Cl into water to which a certain volume of 4 M caustic solution was added to increase the pH to 12; the resulting solution had a caustic concentration of 0.08 M. This feed solution was introduced from a 5 L s. steel Millipore pressure vessel by a Micropump (Ismatec BVP-Z) in crossflow over the outside of the hollow fibers, while the sulfuric acid strip solution was simultaneously introduced from a similar reservoir via the tube side of the module. The concentration of the sulfuric acid solution was 1.3 M. Both flows were in once-through mode. A peristaltic pump was used to introduce the strip sulfuric acid solution into the module via the respective tubing. Tubing used was selected based on the pump-head (Masterflex 7518-60 and 77201-62) and resistance to the chemicals intended to be passed through them. Runs were made for four inlet NH_3 concentrations, 451, 610, 979, 1233 ppm for a few feed flow rates.

A pH meter was used for making pH measurements while determining the pH of the feed solution. The pH probe (Orion 8102BNUWP) was calibrated between −0.91 and 14 by using three buffer solutions provided by the manufacturer as well as sulfuric acid and sodium hydroxide standards prepared in the laboratory. The high performance ammonia gas ion selective electrode (Orion 9512HPBNWP) was calibrated using a ThermoScientific Orion Dual Star pH/ISE (Orion™ 2115001) meter with attached pH probe, a few standard solutions and Ionic Strength Adjuster (ISA, Fisher) in the laboratory. The high performance ammonia gas ion-selective electrode connected to the meter was immersed in the samples and the ppm values of NH_3 were read from the meter.

For the MiniModule™, ammonia-containing feed solution was introduced from a 5L s. steel Millipore reservoir via the bores of the microporous hydrophobic hollow fibers, while the sulfuric acid strip solution was simultaneously introduced via the shell side of the module in an once-through fashion (Fig. 2). The pH of the feed was raised to 11 to convert the unionized ammonia species (NH_4^+) to NH_3 gas by adding a certain volume of 4 M NaOH to the reservoir. The sulfuric acid strip solution of 1.3 M concentration was supplied to the module in the manner described earlier for the Micromodule™. However, in this case, the NH_4Cl feed solution was introduced into the module by a peristaltic pump. Consequently, NH_3 gas diffused through the gas filled pores of the fibers to the H_2SO_4 solution. Runs were made at seven different inlet ammonia concentrations, 38, 98, 355, 748, 897, 933, 1365 ppm and a few flow rates.

Table 1
Information on hollow fiber membranes and three different membrane modules.

Module	1 × 5.5 MiniModule™	0.5 × 1 MicroModule™	10 × 28 LiquiCel®
Number of fibers, N	2300	700	224,000
Porous polypropylene hollow fiber type	X-50	X-50	X-50
Effective module length, L (cm)	11.5	3	61
Effective fiber length, W (cm)	–	3	–
Inner/Outer radius of large cartridge, R_{ci}/R_{co} (cm)	–	–	5.7/12.25
Membrane surface area (cm^2)	1828[c]	98.97[c]	1,300,000[d]
Fractional open area for flow of liquid in radial plane f_x	–	–	0.37
Packing fraction of hollow fibers in the module, f_p	–	–	0.43
Hollow fiber membrane dimensions and properties			
Inner radius, R_i (cm)	0.011	0.011	0.011
Outer radius, R_o (cm)	0.015	0.015	0.015
Porosity, ε	0.4	0.4	0.4
**Tortuosity, τ	–	–	–
Pore diameter, d_p (cm)	4×10^{-6}	4×10^{-6}	4×10^{-6}

** Various estimates are available.
[c] Calculated.
[d] Module data sheet; hollow fiber ends potted with epoxy in the tube sheet in the MiniModule™ and MicroModule™.

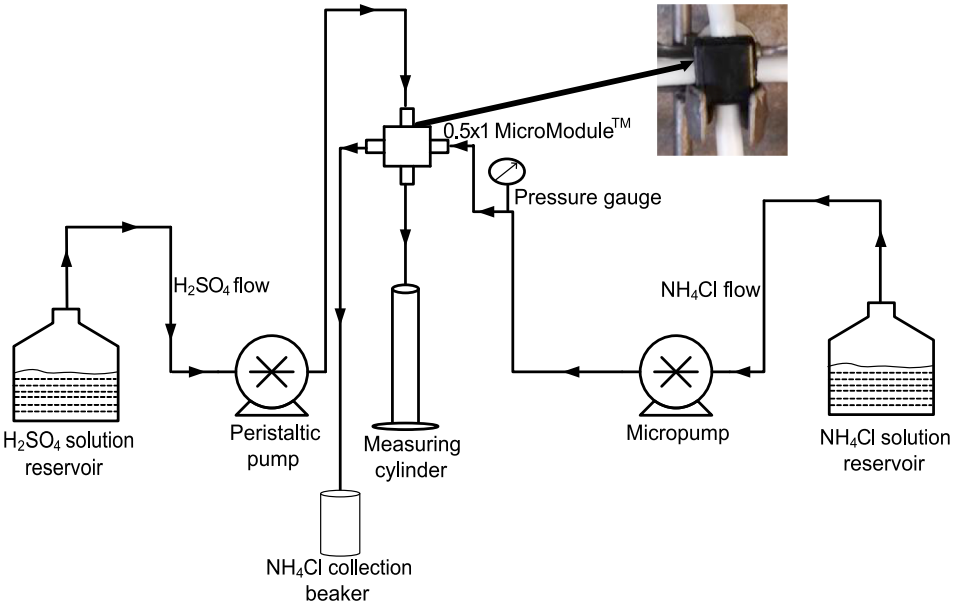

Fig. 1. Schematic of ammonia removal experiments conducted in 0.5 × 1 MicroModule™.

3. Details of models of ammonia transport in various SGM modules

3.1. Minimodule™

In the case of the MiniModule™, the feed solution of ammonium chloride at a pH > 11 was passed through the bore of the hollow fiber membranes potted at two ends of a straight cylindrical module. Fig. 3 shows a single hollow fiber. The flow is along the positive z-direction parallel to the length of the shell as well as the hollow fibers. We assume:

(1) reaction (1a) governing the relation between the NH_4^+ ion and dissolved NH_3 is at equilibrium;
(2) we have a dilute solution of water in great excess;
(3) the sulfuric acid concentration is high enough to assume negligible mass transfer resistance.

Other assumptions are listed below. Almost all of the ammonia will be present as dissolved ammonia gas in the feed due to the high pH; the feed liquid velocity in +ve z direction is v.

$$NH_3(aq) + H_2O \rightleftarrows NH_4^+(aq) + OH^-(aq) \quad (1a)$$

The reaction equilibrium constant K is related to the concentrations of NH_3 gas (C_1), NH_4^+ ion (C_2) and OH^- ion (C_3) by

$$K = \frac{C_2 C_3}{C_1} \quad (1b)$$

The total concentration of ammonia C is the sum of C_1 and C_2

$$C = C_1 + C_2 \quad (2)$$

The total ammonia flux (J) may be expressed as the product

$$J = k_o(C - C^{eq}) \quad (3)$$

where k_o is the overall ammonia transfer coefficient and C^{eq} is its

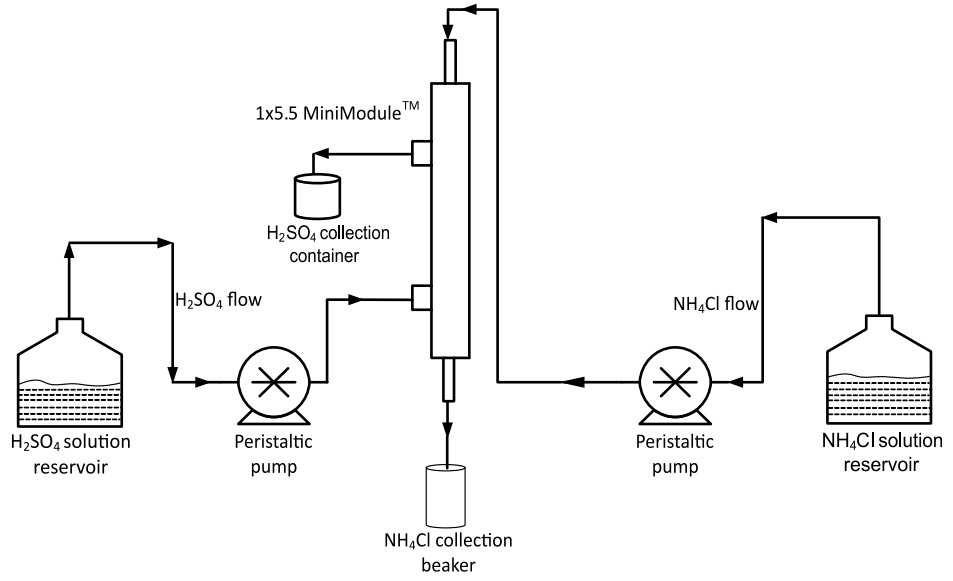

Fig. 2. Schematic of ammonia removal experiments conducted in 1 × 5.5 MiniModule™.

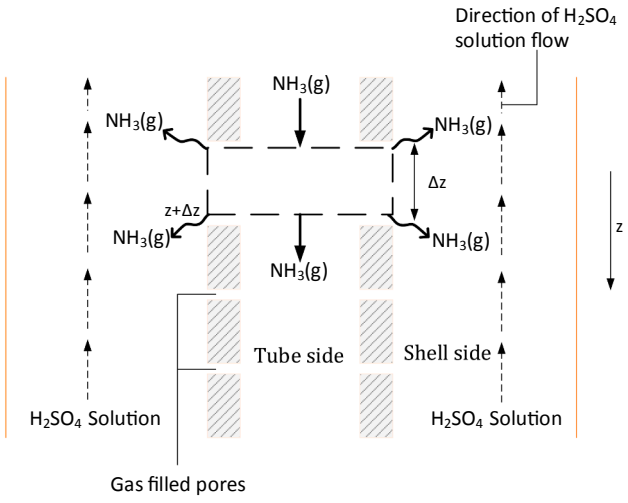

Fig. 3. Control volume for ammonia transport in a single hollow fiber in a 1 × 5.5. MiniModule™.

concentration in the ammonia reabsorption side where due to excess to H_2SO_4, C^{eq} is assumed negligible.

Thus,

$$C^{eq} = 0 \tag{4a}$$

and

$$J = k_o C \tag{4b}$$

A molar balance on total ammonia over a control volume of length Δz in the lumen of one single hollow fiber shown in Fig. 3 is now carried out.

Assumption (4): Steady-state flow of NH_3 – containing feed solution through the fiber bore of cross-sectional area A_c:

$$(vC|_z - vC|_{z+\Delta z})A_c = \pi d_i k_O C \Delta z \tag{5a}$$

$$Lim_{\Delta z \to 0} \frac{(vC|_z - vC|_{z+\Delta z})}{\Delta z} = \frac{\pi d_i k_O C}{A_c} \tag{5b}$$

$$-\frac{d(vC)}{dz} = \frac{\pi d_i k_O C}{A_c} \tag{5c}$$

Assumption (5): $v \neq F(z)$

Therefore,

$$-\frac{dC}{dz} = \frac{\pi d_i k_O C}{A_c v} \tag{5d}$$

Integrating this equation along the fiber length L leads to

$$-\int_{C_o}^{C_{out}} \frac{1}{C} dc = \frac{\pi d_i}{A_c v} \int_0^L k_o dz \tag{6a}$$

for the boundary conditions

Hollow fiber inlet, @ z = 0, C = C_o

Hollow fiber exit, @ z = L, C = C_{out}.

Thus, we get a mass transfer equation for ammonia transport in one hollow fiber:

$$\ln\left(\frac{C_o}{C_{out}}\right) = \frac{\pi d_i \int_0^L k_o dz}{A_c v} \tag{6b}$$

For N hollow fibers in a module, the relation continues to be

$$\ln\left(\frac{C_o}{C_{out}}\right) = \frac{\pi d_i \int_0^L k_o dz}{A_c v} \tag{7a}$$

except v is related to Q, the volumetric flow rate of feed through the bores of N fibers by

$$v = \frac{Q}{A_c N} \tag{7b}$$

The overall mass transfer resistance may be expressed as the sum of three resistances, those due to the liquid film on the feed side ($1/k_f$), the membrane resistance ($1/k_m$) and due to that on the sulfuric acid side ($1/k_s$). We neglect the resistance on the sulfuric acid side; further, the membrane resistance is independent of axial location coordinate, z, whereas the liquid film coefficient is not:

$$\frac{1}{k_s} \simeq 0;\ k_m \neq F(z);\ k_f = F(z) \tag{8}$$

$$\frac{1}{k_o} = \left(\frac{1}{k_f} + \frac{1}{k_m} + \frac{1}{k_s}\right) \simeq \left(\frac{1}{k_f} + \frac{1}{k_m}\right) \tag{9a}$$

The liquid film coefficient may be expressed as a function of axial coordinate z via Leveque equation [26] as long as Graetz number is > 400 [27] which holds here. Therefore,

$$k_f = F(z) = \frac{1.077 D_i^{2/3} d_i^{-1/3} \nu^{1/3}}{z^{1/3}} \qquad \text{[Leveque(expanded)]} \tag{9b}$$

The membrane mass transfer coefficient k_m can be described by [12]

$$k_m = \frac{D_{g,e}\left(\frac{\varepsilon}{\tau}\right)}{R_i \ln(R_o/R_i)}\left(\frac{H_{eff}}{RT}\right) \tag{9c}$$

where $D_{g,e}$ is the diffusion coefficient of ammonia in the membrane pores; the membrane has a porosity of ε and a pore tortuosity of τ. H_{eff} is the effective Henry's law constant; R_i and R_o are the inner and outer radius of the hollow fibers respectively. Since the pore diameter, d_p, is less than 10^{-7} m, estimate of the mean free path of NH_3 in air suggests Knudsen diffusion to be valid (see Table 2): Knudsen diffusivity $D_{g,k}$ may be used for gas phase diffusivity, $D_{g,e}$

$$D_{g,e} \approx D_{g,k} = \frac{d_p}{3}\sqrt{\frac{8RT}{\pi M_i}} \tag{9d}$$

The effective value H_{eff} of Henry's constant of NH_3 in a feed solution of ionic strength I and molar concentration C_i of various species in solution is related to that in water H by the following relation where the factor h has contributions from cations (h_+), anions (h_-) and the gas species present (h_G) (see the values of each for different species in [28]):

$$Log_{10}(H_{eff}/H) = hI \tag{10a}$$

$$h = h_+ + h_- + h_G. \tag{10b}$$

and

$$I = \frac{1}{2}\sum C_i z_i^2 \tag{10c}$$

One can use result (7a) to predict C_{out} at a given flow rate after incorporating the z-dependent expression for k_f from Eq. (9b). The only item needed for prediction is the membrane tortuosity τ whose value can be assumed based on literature [31,32].

Table 2
Properties of ammonia and other quantities for SGM module studies at 298.15 K.

*Henry's constant in H_2O, H (Pa/M)	1695
**Diffusion coefficient in H_2O, D_i (cm^2/s)	1.64×10^{-5}
Knudsen diffusion coefficient in air, $D_{g,e}$ (cm^2/s)	8.12×10^{-2}
*[1]Membrane mass transfer coefficient for τ = 2.8, k_m (cm/s)	0.0024
*[1]Membrane mass transfer coefficient for τ = 6.4, k_m (cm/s)	0.0010

*Sander (2015) [29]; **He et al. [13]; ** Semmens et al. [10]; ** Cussler [30]; *[1] [31,32].

One can alternately employ experimental data and the model to estimate k_m for use in calculating model results for the MicroModule™ and the much larger 10 × 28 modules.

3.2. MicroModule™

In general, for a liquid phase mass transfer coefficient, Sherwood number is related functionally to the Reynolds number and Schmidt number via the equation:

$$\frac{k_f d_F}{D_i} = a\left[\frac{d_F v_x \rho}{\mu}\right]^b \left[\frac{\mu}{\rho D_i}\right]^c \tag{11a}$$

This can be rewritten as

$$k_f = \Lambda v_x^b \tag{11b}$$

$$k_f = \Lambda \frac{Q_x^b}{A_{fc}^b} \tag{11c}$$

Here v_x is the velocity of the feed liquid which is in crossflow over the hollow fibers (Fig. 4) through the bore of which sulfuric acid solution flows, A_{fc} is the actual flow cross-section of the feed liquid flow in between the hollow fibers with a velocity v_x and Λ is defined by

$$\Lambda = \frac{a}{d_F^{1-b}}\left[\frac{\rho}{\mu}\right]^{b-c} [D_i]^{1-c} \tag{11d}$$

The MicroModule™ has a few layers of hollow fibers one after another in the x direction with the feed liquid in crossflow (Fig. 4). The total number of fibers in the module is N and the number of fiber layers in x-direction is n_f. A differential molar balance on ammonia over one layer of fibers in x direction for negligible sulfuric acid side resistance leads to (for a surface area dA_T)

$$-QdC = k_o dA_T C \tag{12a}$$

$$-\frac{dC}{C} = \frac{k_o \pi d_F W \frac{N}{n_f}}{Q} \tag{12b}$$

where W is the length of hollow fibers perpendicular to the shell-side mean flow direction. Correspondingly, for n_f layers of hollow fibers, we have:

$$-\int_{C_o}^{C_{out}} \frac{dC}{C} = \frac{k_o \pi d_F WN}{Q} \tag{12c}$$

Therefore,

$$\ln\left(\frac{C_o}{C_{out}}\right) = \frac{k_o \pi d_F WN}{Q} \tag{13}$$

Combining (9a), (11c) and (13), we get

$$\ln\left(\frac{C_o}{C_{out}}\right) = \pi d_F WN\left[\frac{1}{\frac{A_{fc}^b Q^{1-b}}{\Lambda} + \frac{Q}{k_m}}\right] \tag{14a}$$

The separation efficiency, E, can be defined in terms of the incoming feed concentration, C_o, and the outlet concentration, C_{out}, by the following equation:

$$E = 1 - \frac{C_{out}}{C_o} \tag{14b}$$

Therefore,

$$\ln\left(\frac{1}{1-E}\right) = \pi d_F WN\left[\frac{1}{\frac{A_{fc}^b Q^{1-b}}{\Lambda} + \frac{Q}{k_m}}\right] \tag{14c}$$

An estimate of the experimentally observed overall mass transfer coefficient k_o may be determined from experimental results from the following equation:

$$k_o = \frac{Q}{A_T} ln\left(\frac{1}{1-E}\right) \tag{14d}$$

Two quantities are unknown in Eq. (14c) if we assume k_m to be known. We do not know the power 'b' of the crossflow velocity v_x and the value of the coefficient 'a' in Eq. (11a). Correspondingly, 'b' and Λ are unknown and are needed to predict E. The power 'c' in Eq. (11a) is usually 1/3 for liquid systems of interest. Guidance is available in literature on what the value of 'b' is likely to be in simple crossflow across a bank of hollow fibers developed in studies with CO_2 transport [22,25].

3.3. 10 × 28 industrial scale module

A schematic of the flow pattern and module configuration in the two-zone contactor is shown in Fig. 5. The local radial velocity v_r can be written in terms of the feed volumetric flow rate Q in the following fashion where f_x is the fractional open area for flow of liquid in the radial direction inward or outward and (L/2) is the active length of the fiber in each zone [23] (see Table 1 for information on f_x):

$$Q = \frac{2\pi r L v_r f_x}{2} \tag{15a}$$

Similar to expression (11b) for k_f, we have k_f written in terms of v_r as follows:

$$k_f = \Lambda v_r^b \tag{15b}$$

Combining (15a) and (15b), we get k_f in terms of Q:

$$k_f = \Lambda \frac{Q^b}{(\pi f_x L)^b r^b} \tag{15c}$$

Following Sengupta et al. [23], the number of hollow fibers inside a

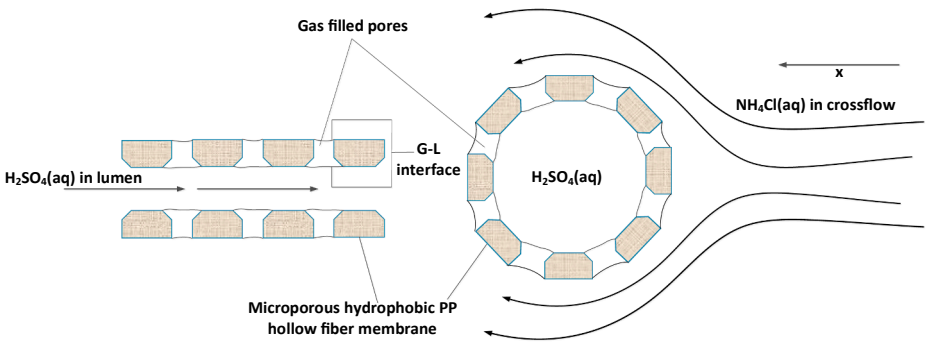

Fig. 4. Cross flow of feed solution around a single hollow fiber for ammonia transport in a 0.5 × 1 MicroModule™. G-L – gas–liquid interface.

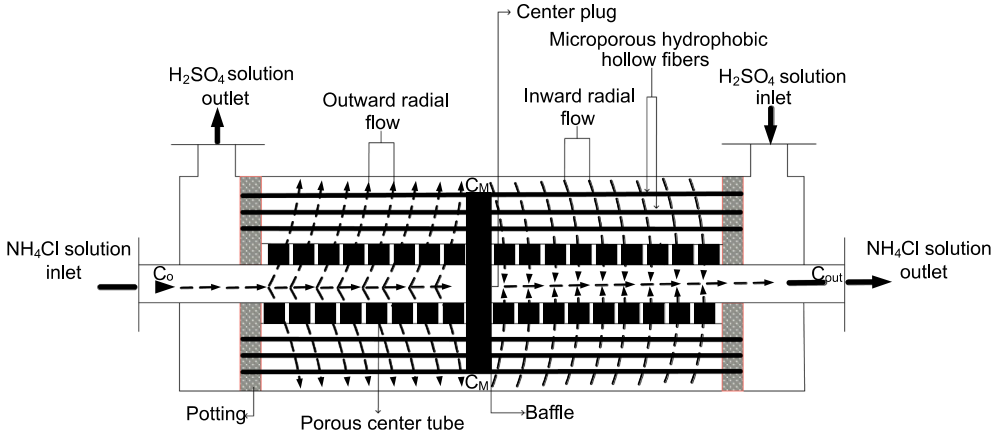

Fig. 5. Schematic for flow directions of two streams in a single 10 × 28 LiquiCel® hollow fiber module with two zones on two sides of the central baffle.

differential slice, dN, can be written in terms of the hollow fiber packing fraction, f_p, as follows (Table 1 provides f_p value):

$$dN = \frac{f_p 2\pi r dr}{\frac{\pi d_F^2}{4}} = \frac{8 f_p}{d_F^2} r dr \tag{16a}$$

The corresponding mass transfer area, dA_T, based on the hollow fiber outside diameter (OD) is given by:

$$dA_T = \frac{\pi d_F L dN}{2} = \frac{4\pi f_p L}{d_F} r dr \tag{16b}$$

Here, the length of the hollow fibers is half the active length L of the module. Combining Eqs. (9a), (12a), (15c) and (16b) we get:

$$\frac{dC}{C} = \frac{-4\pi f_p L}{d_F Q}\left[\frac{r dr}{\frac{(\pi f_x L)^b r^b}{\Lambda Q^b} + \frac{1}{k_m}}\right] \tag{17a}$$

$$\frac{dC}{C} = \frac{-4\pi f_p L}{d_F}\left[\frac{r dr}{\frac{(\pi f_x L)^b r^b Q^{1-b}}{\Lambda} + \frac{Q}{k_m}}\right] \tag{17b}$$

By integrating relation (17b) from the center to the periphery, we get:

$$-\int_{C_0}^{C_M} \frac{dC}{C} = \frac{4\pi f_p L}{d_F} \int_{R_{ci}}^{R_{co}} \frac{r dr}{\frac{(\pi f_x L)^b r^b Q^{1-b}}{\Lambda} + \frac{Q}{k_m}} \tag{18a}$$

Where,

C_o is the average concentration of NH_3 in the feed solution, and C_M is the average concentration of NH_3 leaving the first zone of the contactor and entering the second zone.

Similarly, for the second half of the module we have,

$$-\int_{C_M}^{C_{out}} \frac{dC}{C} = \frac{4\pi f_p L}{d_F} \int_{R_{ci}}^{R_{co}} \frac{r dr}{\frac{(\pi f_x L)^b r^b Q^{1-b}}{\Lambda} + \frac{Q}{k_m}} \tag{18b}$$

By combining the integrals of (18a) and (18b), we get:

$$ln\left(\frac{C_o}{C_{out}}\right) = \frac{8\pi f_p L}{d_F} \int_{R_{ci}}^{R_{co}} \frac{r dr}{\frac{(\pi f_x L)^b r^b Q^{1-b}}{\Lambda} + \frac{Q}{k_m}} \tag{19}$$

Defining the left-hand side of (19) in terms of E we get:

$$ln\left(\frac{1}{1-E}\right) = \frac{8\pi f_p L}{d_F} \int_{R_{ci}}^{R_{co}} \frac{r dr}{\frac{(\pi f_x L)^b r^b Q^{1-b}}{\Lambda} + \frac{Q}{k_m}} \tag{20}$$

Similar to Eq. (14d), from relation (20), one can estimate the overall mass transfer coefficient for the whole module as follows:

$$k_o = \frac{Q}{A_T} ln\left(\frac{1}{1-E}\right) \tag{21}$$

Here A_T is the total surface area available for mass transfer based on the outside diameter of the hollow fibers. The unknown quantities in this result are as in the Micromodule™ analysis: coefficient 'a' in mass transfer correlation (11a) and the power 'b' of Reynolds number (assuming that power 'c' in the same correlation is 1/3); further, k_m is assumed known from the two studies made here. For the large commercial modules of 10x28 dimensions, the value of 'a' has been determined by Zheng et al. [24] to be 2.15. The power 'b' for such modules appear to be in a small range around 0.42 [23,24].

4. Results and discussion

4.1. MiniModule™

The experimental results from studies with the MiniModule™ will be presented first (see Figs. 6a and 6b). The results will then be compared with the predictions from the analysis carried out in Section 3.1. Specifically, the observed values of the outlet concentration C_{out} can be compared with the predicted values shown by the dashed lines in

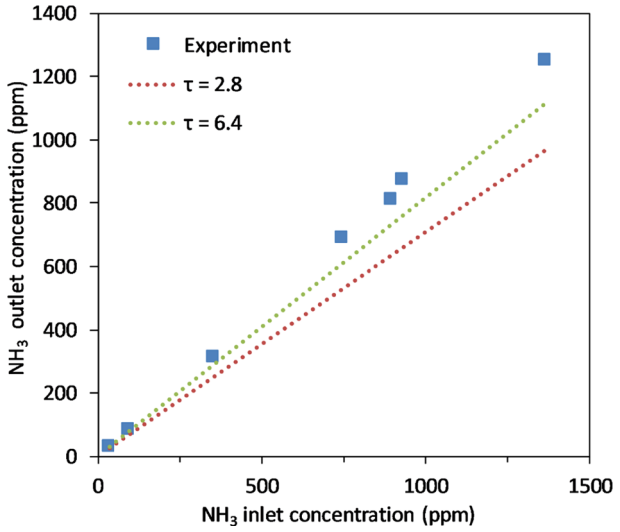

Fig. 6a. Outlet NH_3 concentration dependence on inlet NH_3 concentration for a feed flow rate of 425 ml/min (± 2.6%) in 1 × 5.5 MiniModule™. The dashed lines illustrate model predictions for two values of the membrane tortuosity, τ.

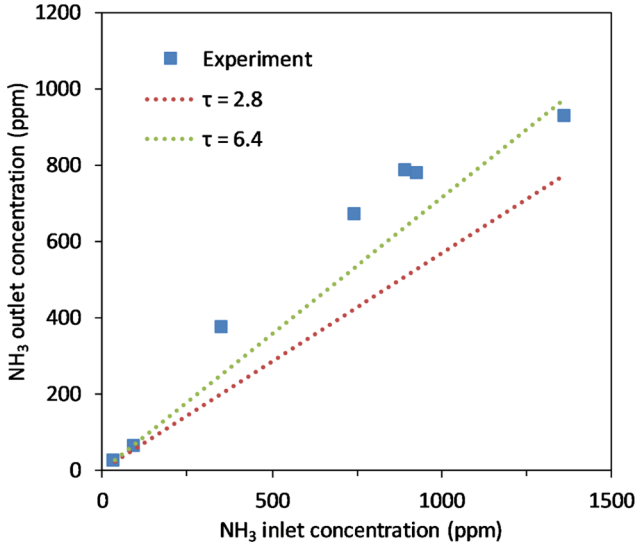

Fig. 6b. Outlet NH_3 concentration dependence on inlet NH_3 concentration at 239 ml/min (± 2.9%) feed flow rate in 1 × 5.5 MiniModule™.

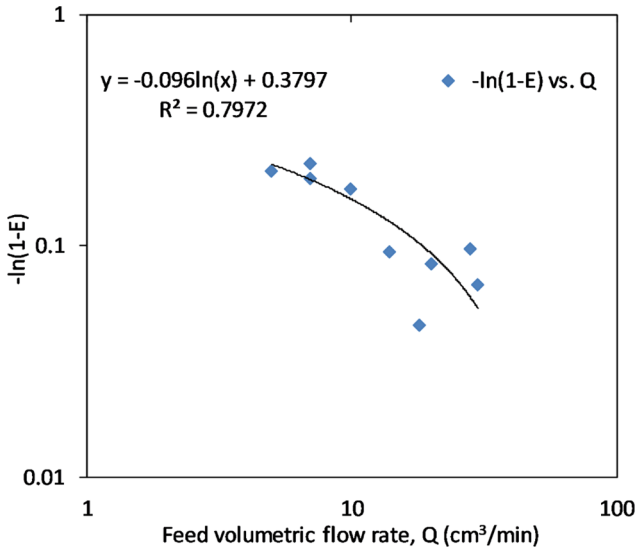

Fig. 7a. Feed flow rate effect on ammonia separation efficiency in 0.5 × 1 MicroModule™.

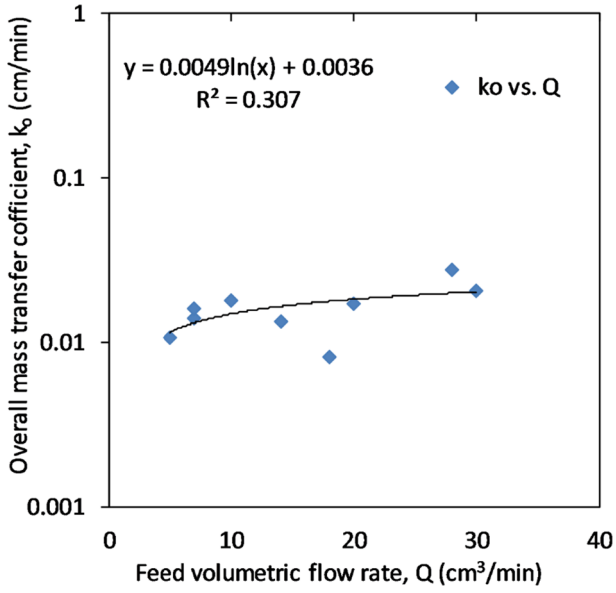

Fig. 7b. Volumetric feed flow rate dependence of experimental overall ammonia mass transfer coefficient in 0.5 × 1 MicroModule™.

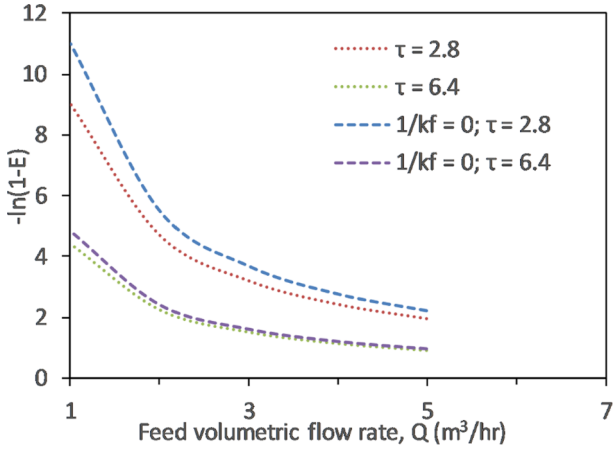

Fig. 8. Volumetric feed flow rate dependence of ammonia separation efficiency in a single 10 × 28 LiquiCel® module for two different membrane tortuosities, τ = 2.8 (k_m = 0.0024 cm/s) and τ = 6.4 (k_m = 0.0010 cm/s).

Figs. 6a and 6b. Fig. 6a is for an average feed flow rate of 425 ml/min. Fig. 6b is for an average feed flow rate of 239 ml/min. There were seven different inlet ammonia concentrations. The values of the parameters used to carry out calculations for the model represented by Eq. (7a) are provided in Table 2; this equation allows estimation of C_{out}. Estimates of tortuosity factor, τ, were developed from the following two correlations in literature ((Mackie et al. [31]); (Iversen et al. [32])) for the values of porosity for the hollow fiber membranes used:

$$\frac{\tau}{\varepsilon} = \frac{(2-\varepsilon)^2}{\varepsilon^2} \tag{22a}$$

$$\tau = \frac{1}{\varepsilon} \tag{22b}$$

It appears that at higher inlet concentrations, the model predicts values lower than those experimentally observed. But a much higher tortuosity factor of τ = 6.4 resulting from Mackie et al. [31] correlation and close to that experimentally observed by Iversen et al. [32] with Celgard 2400 and 2500 membranes appears to bring the predictions significantly closer to the experimental data. Lower τ values have been used and suggested for Celgard hollow fiber membranes, 3 in [10] and 2.6 in [33]; so an average of 2.8 was used. Each data point represents one measurement in the MiniModule™ only for a given experiment; the experiments were repeated. On the other hand, the average of three measurements represents a data point in a given MicroModule™ experiment described below. The relation (22b) apparently is a better fit for high porosity values characterized by quite open membranes; the current hollow fiber membranes have much lower porosity closer to those of Celgard 2400/2500.

Additional sources of discrepancy between the MiniModule™ data and the model predictions are likely to be due to the following. Henry's constant for ammonia-water system was found by Calingaert et al. [34] to be decreasing with increasing ammonia concentration. Consequently, the actual membrane resistance which includes Henry's constant increases with increasing inlet NH_3 concentration and becomes significantly higher than the calculated membrane resistance; this would yield higher experimental NH_3 concentrations than the predicted values. Variation in the feed flow rate during measurements did not lead to significant changes in the predicted outlet concentrations. However, coarse reading by the high performance ammonia gas ion-selective electrode can contribute to measurement errors.

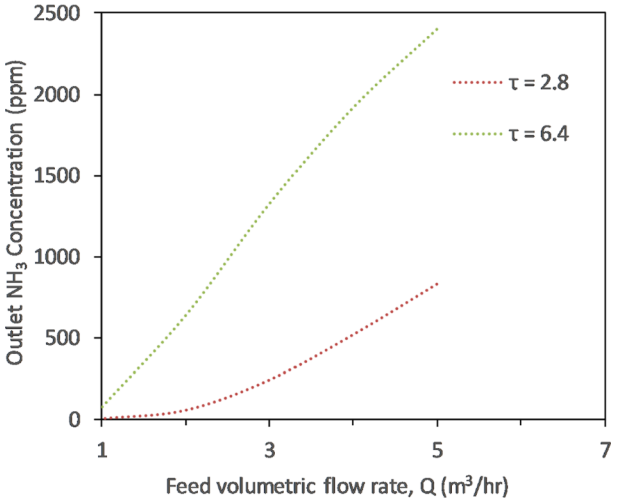

Fig. 9. Predicted outlet ammonia concentration against feed volumetric flow rate variation in a single 10 × 28 LiquiCel® module for two different membrane tortuosities, τ = 2.8 (k_m = 0.0024 cm/s) and τ = 6.4 (k_m = 0.0010 cm/s), and 6000 ppm inlet concentration.

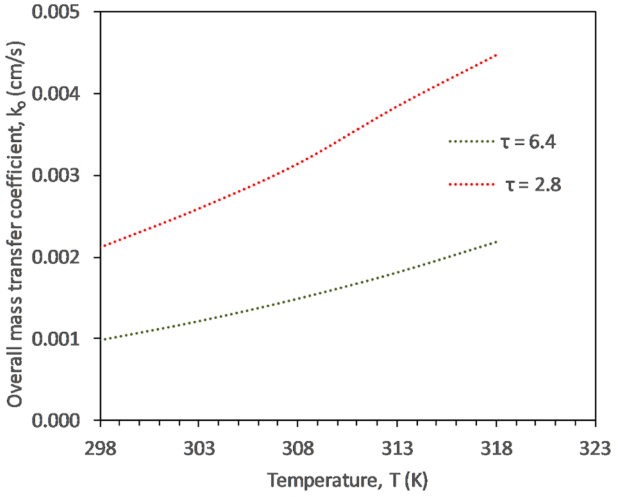

Fig. 10a. Temperature dependence of predicted overall mass transfer coefficient for ammonia in 10 × 28 LiquiCel® module for τ = 2.8 and τ = 6.4 at Q = 5 m^3/h.

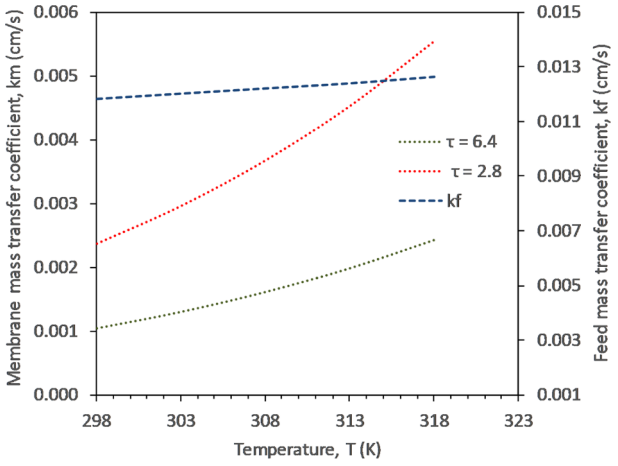

Fig. 10b. Temperature dependence of predicted values of membrane mass transfer coefficient and feed phase mass transfer coefficient for ammonia in 10 × 28 LiquiCel® module for τ = 2.8 and τ = 6.4 at Q = 5 m^3/h.

4.2. MicroModule™

The experimental results from the data obtained with the MicroModule™ will be illustrated now via Figs. 7a and 7b. Fig. 7a provides a log-log plot of the experimental data in the form of −ln (1 − E) against feed solution flow rate. Eq. (14c) illustrates the predicted relation for this behavior. The experimental k_o values have been plotted against the feed volumetric flow rate in a semi-log plot in Fig. 7b. Eq. (9a) for the overall mass transfer coefficient k_o can be used to obtain theoretical estimates for the device based on Eq. (11a) for k_f and an appropriate value of k_m.

There are a number of unknown parameters in Eq. (14c) as well as (11a): b, Λ; the coefficient a in Eq. (11a) is hidden in the parameter, Λ. Further, a value of k_m is needed as well. One can assume various values of the first two parameters based on literature guidance and carry out a sensitivity analysis in terms of predicting the outlet concentration or (1 − E). Tables S.1a and S.1b (see supplementary information) provide the results of such an analysis based on two k_m values identified in Table 2. It appears that a value of power 'b' of Reynolds number between 0.3 and 0.43 provides reasonable estimates of the outlet concentrations (Eq. (23)) for the larger value of k_m (corresponding to a τ value of 2.8). For the smaller value of k_m (corresponding to a τ value of 6.4), the range of b changes a bit. Such a range of values of b is often observed in correlations of k_f for crossflow membrane contactors [22–25] including the large-scale Liqui-Cel® contactors. Correspondingly, coefficient 'a' changes also.

Estimates of b were obtained based on the criteria that the most sensitive set of predicted average NH_3 concentrations (1008–1107 ppm) are greater than corresponding average outlet concentration obtained from experiment (1013 ppm) and less than the first outlet concentration (1050 ppm) at a particular NH_3 feed concentration and flow rate. Therefore, by assuming a τ value of 2.8, we have b ranging between 0.30 and 0.43 and the correlation for film transfer coefficient in cross-flow of the feed liquid phase in MicroModule™ may be represented as

$$Sh = 0.02Re^{0.30-0.43}\,Sc^{0.33} \tag{23}$$

Similarly, estimates of b were obtained based on the aforementioned criteria for the smaller k_m. However, we have 'b' ranging from 0.33 to 0.47 at a τ value of 6.4. More interestingly, at this tortuosity value, we have two values of 'a'. One corresponds to 'b' values ranging from 0.33 to 0.35 (Table S.1b), while the other corresponds to 'b' values ranging from 0.36 to 0.47. Therefore, similar to Eq. (23) the film mass transfer coefficient in cross-flow of the feed liquid phase in MicroModule™ may be represented as:

$$Sh = 0.03Re^{0.33-0.35}\,Sc^{0.33} \tag{24a}$$

$$Sh = 0.02Re^{0.36-0.47}\,Sc^{0.33} \tag{24b}$$

4.3. Large 10 × 28 module

We will now consider the modeling results for the large 10 × 28 LiquiCel® module. The configuration here involves once-through flow of feed liquid solution in cross-flow through the shell-side and sulfuric acid solution flow through the tube-side such that the dissolved concentration of ammonia in it is essentially zero. A plot of the type shown in Fig. 7(a) which is independent of feed concentration will be used. Fig. 8 shows such a plot representing the behavior of −ln (1 − E) from Eq. (20) as a function of the feed solution volumetric flow rate Q for two membrane resistances. This may be utilized to predict the performance of a 10 × 28 LiquiCel® module for any incoming ammonia concentration. This plot includes additional information such as what happens if one assumes that there is essentially no liquid phase mass transfer resistance. It is clear that k_m dominates mass transfer and k_f has a very limited role for highly soluble gases like like ammonia. For the higher tortuosity case, the membrane resistance appears to be completely

controlling.

Ulbricht et al. [5] employed two such modules in series to remove ammonia from a solution in a tank with a feed concentration of around 6000 ppm. They employed batch recirculation mode at a feed flow rate of 5 m^3/h with the feed pH being sufficiently high. Such a mode of operation is useful if in one pass the feed solution is stripped substantially of the feed ammonia so that when the treated feed solution is exiting the module and is fed back into the feed tank, it reduces the ammonia burden in the tank. Using Eq. (20), one can determine what is the outlet concentration from the first module (which becomes the feed for the second module) and that from the second module. Fig. 9 illustrates the flow rate dependence of the outlet concentration from one module for an inlet concentration of 6000 ppm. Such plots are useful for optimization and operational design of the SGM-based membrane strippers.

The operational temperature in ammonia removal can vary depending on the source water temperature. Due to the strong temperature dependence of various relevant quantities, it is useful to determine how the predicted performances vary with temperature. Fig. 10a illustrates the predicted values of the overall mass transfer coefficient k_o as a function of feed temperature for two values of membrane transfer coefficients, 0.0010 cm/s and 0.0024 cm/s respectively. This was obtained by varying the liquid phase diffusivity of ammonia [35], liquid phase viscosity, Henry's law constant for ammonia [29] and gas phase diffusivity of ammonia as a function of temperature. This figure illustrates the considerable utility of stripping the ammonia at a somewhat higher feed feed solution temperature. This figure also illustrates the strong effect of membrane transfer coefficient on the overall mass transfer rate. It is as if k_m controls k_o as was indicated in Fig. 8.

It is instructive to look further at the issue of temperature dependence. For this large module, consider the effect of temperature on two different components of the overall mass transfer coefficient k_o namely, k_m and k_f. Fig. 10b illustrates the temperature dependence of k_m for two values of the membrane tortuosity τ. Fig. 10b shows also the variation of k_f with temperature. It is clear that variation of temperature affects k_m drastically. An increase of 20 °C enhances the membrane transfer coefficients by as much as 2.5 times. On the other hand, the same temperature increase enhances the value of k_f by approximately 6.8%.

It is important to recognize that there are uncertainties in the values of the following parameters: coefficient 'a', power 'b' of Reynolds number and the membrane transfer coefficient, k_m. We have used in all model calculations a value of 'a' = 2.15 per Zheng et al. [24]. A reduction in the value of this parameter 'a' will however reduce the value of the overall mass transfer coefficient k_o only by a very limited amount. That is one reason to avoid a detailed CFD-based modeling of the shell-side flow field.

There are a number of other issues not considered here. The water vapor partial pressure on the sulfuric acid side is likely to be lower than that on the feed side resulting in some water vapor transport through the membrane pores to the sulfuric acid side. This was observed by Ulbricht et al. [5]. This may affect the value of k_m with a multicomponent transport situation between ammonia, air, and water vapor. It will also increase the feed ammonia concentration and introduce predictive uncertainty. The acid-base reaction at the receiving gas-liquid interface will be exothermic and may lead to local increase in temperature which will affect Henry's law constant and therefore the reabsorption rate of ammonia. An aspect that has not been considered yet involves the assumption that the sulfuric acid side resistance is negligible. Our experiments employed 1.3 M sulfuric acid solution. We do not foresee any problem with such an assumption with this level of sulfuric acid. However, during actual large-scale utilization of this technique directed towards producing a usable solution of ammonium sulfate, the pH of the sulfuric acid side may be around 3–4. How this will reduce the mass transfer coefficient has not been considered.

5. Concluding remarks

Experimental studies were made to determine the rate of ammonia transfer from a feed solution at a high pH to a sulfuric acid solution through the pores of porous non-wetted hydrophobic hollow fiber membranes. Two module configurations were utilized for ammonia transfer via a SGM. In a MiniModule™, the feed solution was passed through the hollow fiber bore in laminar flow so that the mass transfer was amenable to easier modeling since the sulfuric side resistance on the shell side was negligible. Comparison with the experimental data allowed development of estimates of the membrane mass transfer coefficient. In a MicroModule™ with crossflow of feed solution over the outside of the hollow fibers, a reasonable description of the shell side mass transfer coefficient in crossflow was developed; the description depended somewhat on the membrane mass transfer coefficient used. A model was developed also for ammonia transport in large 10 × 28 Liqui-Cel® modules which have crossflow of the feed solution over the outside of the fibers. The overall mass transfer coefficient depends here strongly on the membrane resistance estimated earlier from MiniModule™ studies. The model developed for the large module illustrates how ammonia removal depends on the feed flow rate and temperature.

Acknowledgments

The authors gratefully acknowledge support for this research from the NSF Industry/University Cooperative Research Center for Membrane Science, Engineering and Technology that has been supported via two US NSF Awards IIP1034710 and IIP-1822130. We are grateful to 3M Corporation for donating a number of MicroModules™ and MiniModules™ to our research.

Appendix A. Supplementary material

Supplementary data to this article can be found online at https://doi.org/10.1016/j.seppur.2019.04.074.

References

[1] J. Plautz, Piercing the haze, Science 361 (6407) (2018) 1060–1063.
[2] F. Ozyonar, B. Karagozoglu, M. Kobya, Air stripping of ammonia from coke wastewater, Int. J. Eng. Sci. Technol. 15 (2012) 85–91.
[3] T.C. Jorgensen, L.R. Weatherley, Ammonia removal from wastewater by ion exchange in the presence of organic contaminants, Water Res. 37 (2003) 1723–1728.
[4] J.L. Campos, J.M. Garrido-Fernandez, R. Mendez, J.M. Lema, Nitrification at high ammonia loading rates in an activated sludge unit, Bioresour. Technol. 68 (2) (1999) 141–148.
[5] M. Ulbricht, G. Lakner, J. Lakner, K. Belafi-Bako, TransMembraneChemiSorption of ammonia from sealing water in Hungarian powder metallurgy furnace, Desalin. Water Treat. 75 (2017) 253–259.
[6] J.M. Wright, W.T. Lindsay, Jr., T.R. Druga. USAEC Comm. R&D report WAPD TM-204. 32 pp (1961).
[7] C.N. Sawyer, P.L. McCarty, G.F. Parkin, Chemistry for environmental engineering and science, 5th ed., McGraw-Hill Education, New York, NY, 2002.
[8] M. Imai, S. Furusaki, T. Miyauchi, Separation of volatile materials by gas membranes, I&EC Proc. Des. and Dev. 21 (1982) 421–426.
[9] Zhang Qi, E.L. Cussler, Hollow fiber gas membranes, AIChE J. 31 (1985) 1548–1553.
[10] M.J. Semmens, D.M. Foster, E.L. Cussler, Ammonia removal from water using microporous hollow fibers, J. Membr. Sci. 51 (1990) 127.
[11] C.F. Kenfield, R. Qin, M.J. Semmens, E.L. Cussler, Cyanide recovery across hollow fiber gas membranes, Environ. Sci. Technol. 22 (1989) 1151–1155.
[12] Y.J. Qin, J.M.S. Cabral, S.C. Wang, Hollow-fiber gas-membrane process for removal of NH_3 from solution of NH_3 and CO_2, AIChE J. 42 (1996) 1945–1956.
[13] J. He, H. Liu, P. Shan, K. Zhang, Y. Qin, L. Liu, Supported-gas-membrane process for removal and recovery of aliphatic amines from aqueous streams, Chem. Eng. Sci. 141 (2016) 330–341.
[14] Z. Shen, B. Han, S.R. Wickramasinghe, Cyanide removal from wastewater using gas membranes: Commercial scale study, Water Environ. Res. 76 (1) (2004) 15–22.
[15] B. Han, Z. Shen, S.R. Wickramasinghe, Cyanide removal from industrial wastewaters using gas membranes, J. Membr. Sci. 257 (1–2) (2005) 171–181.
[16] B. Han, Z. Shen, S.R. Wickramasinghe, Fouling and cleaning of gas membranes for cyanide removal, Sep. Sci. Technol. 40 (6) (2005) 1169–1180.
[17] J. Shen, B. Han, S.R. Wickramasinghe, Cyanide removal from industrial

praziquantel wastewaters using integrated coagulation–gas-filled membrane absorption process, Desalination 195 (1–3) (2006) 40–50.
[18] Z. Shen, L. Zhang, S. Mondal, S.R. Wickramasinghe, Suppression of osmotic distillation in gas membrane processes, Sep. Sci. Technol. 43 (15) (2008) 3813–3825.
[19] TB 74, 2009; TB 84, 2015: Membrana, Charlotte, NC, USA.
[20] M.-C. Yang, E.L. Cussler, Designing hollow fiber contactors, AIChE J. 32 (1986) 1910–1916.
[21] S.R. Wickramasinghe, M.J. Semmens, E.L. Cussler, Better hollow fiber contactors, J. Membr. Sci. 62 (3) (1991) 371–388.
[22] D. Bhaumik, S. Majumdar, K.K. Sirkar, Absorption of CO_2 in a transverse flow hollow fiber membrane module having a few wraps of the fiber, J. Membr. Sci. 138 (1) (1998) 77–82.
[23] A. Sengupta, P.A. Peterson, B.D. Miller, J. Schneider, C.W. Fulk Jr., Large-scale application of membrane contactors for gas transfer from or to ultrapure water, Sep. Purif. Technol. 14 (1998) 189–200.
[24] J.-M. Zheng, Z.-W. Dai, F.S. Wong, Z.-K. Xu, Shell side mass transfer in a transverse flow hollow fiber membrane contactor, J. Membr. Sci. 261 (2005) 114–120.
[25] H. Estay, E. Troncoso, R. Ruby-Figueroa, J. Romero, Performance evaluation of mass transfer correlations in the GFMA process: A review with perspectives to the design, J. Membr. Sci. 554 (2018) 140–155.
[26] K.K. Sirkar, Separation of molecules, macromolecules and particles: Principles, phenomena and processes, Cambridge University Press, 2014 p. 110.
[27] A.H.P. Skelland, Diffusional mass transfer, Wiley, New York, 1974 p. 167.
[28] P.V. Danckwerts, Gas-liquid reactions, McGraw-Hill, New York, 1970 p. 18–21.
[29] R. Sander, Compilation of Henry's law constants (version 4.0) for water as solvent, Atmos. Chem. Phys. 15 (2015) 4399–4981.
[30] E.L. Cussler, Diffusion, Cambridge University Press, London, 1984.
[31] J.S. Mackie, P. Meares, The diffusion of electrolytes in a cation-exchange resin membrane I. Theoretical, Proc. R. Soc. Lond. A 232 (1191) (1955) 498–509.
[32] S.B. Iversen, V.K. Bhatia, K. Dam-Johansen, G. Jonsson, Characterization of microporous membranes for use in membrane contactors, J. Membr. Sci. 130 (1–2) (1997) 205–217.
[33] T. Mulukutla, G. Obuskovic, K.K. Sirkar, Novel scrubbing system for post-combustion CO_2 capture and recovery: Experimental studies, J. Membr. Sci. 471 (2014) 16–26.
[34] G. Calingaert, F.E. Huggins Jr., An apparent deviation from Henry's law for the system, ammonia-water, JACS 45 (4) (1923) 915–920.
[35] C.R. Wilke, P. Chang, Correlation of diffusion coefficients in dilute solutions, AIChE J. 1 (2) (1955) 264–270.